Journal of Physics D: Applied Physics

PAPER • **OPEN ACCESS**

Magnetic performance of $SrFe_{12}O_{19}$–$Zn_{0.2}Fe_{2.8}O_4$ hybrid magnets prepared by spark plasma sintering

To cite this article: P Jenuš *et al* 2021 *J. Phys. D: Appl. Phys.* **54** 204002

OPEN ACCESS
IOP Publishing
Journal of Physics D: Applied Physics
J. Phys. D: Appl. Phys. **54** (2021) 204002 (8pp)
https://doi.org/10.1088/1361-6463/abdf96

Magnetic performance of $SrFe_{12}O_{19}$–$Zn_{0.2}Fe_{2.8}O_4$ hybrid magnets prepared by spark plasma sintering

P Jenuš[1], A Učakar[1,2], S Repše[1,2], C Sangregorio[3,4,7], M Petrecca[3,4,7], M Albino[4,5,7], R Cabassi[6], C de Julián Fernández[6,7] and B Belec[6]

[1] Department for Nanostructured Materials, Jožef Stefan Institute, Ljubljana, Slovenia
[2] Faculty for Natural Sciences, University of Ljubljana, Ljubljana, Slovenia
[3] I.C.C.O.M.—CNR, Sesto Fiorentino, Italy
[4] Department of Chemistry, University of Florence, Sesto Fiorentino, Italy
[5] Department of Industrial Engineering, University of Florence, Florence, Italy
[6] Institute of Materials for Electronic and Magnetism- CNR, Parma, Italy
[7] Consorzio INSTM, Florence, Italy

E-mail: petra.jenus@ijs.si

Received 23 September 2020, revised 11 January 2021
Accepted for publication 25 January 2021
Published 1 March 2021

Abstract

In the last few years, significant effort has again been devoted to ferrite-based permanent magnet research due to the so-called rare-earth crisis. In particular, a quest to enhance ferrites maximum energy product, BH_{max}, is underway. Here, the influence of composition and sintering conditions on the microstructure and consequently magnetic properties of strontium ferrite-based hybrid composites was investigated. The powder mixtures consisted of hydrothermally synthesised Sr-ferrite with hexagonally shaped platelets with a diameter of 1 μm and thickness up to 90 nm, and a soft magnetic phase in various ratios. Powders were sintered using a spark plasma sintering furnace. The crystal structure, composition and microstructure of the starting powders and hybrid magnets were examined. Their magnetic properties were evaluated by vibrating sample magnetometer, permeameter and by single-point-detection measurements.

Supplementary material for this article is available online

Keywords: Sr-ferrite, hard–soft composites, SPS, magnetic properties

(Some figures may appear in colour only in the online journal)

1. Introduction

Permanent magnets (PMs) are crucial elements in modern devices and are enabling technologies as they allow storing, delivering and converting energy [1]. Due to their properties, PMs are one of the vital components of the green revolution, playing an essential role in both renewable energy (i.e. in wind turbines there is an 80–650 kg MW^{-1} of PM [2]) and electric mobility (for example, there is 5–10 kg of PM in a single electric car [3]). Apart from wind power and electric vehicles, PMs are also found in electric bikes, acoustic transducers, hard disk drives and many other applications.

In 1960, the PM market underwent a total revolution with the appearance of rare earth (RE) PMs. Their energy products rise to over 240 kJ m^{-3} for SmCo and to over 400 kJ m^{-3} for NdFeB. Since raw materials were abundant for the fabrication of PMs located in non-developed countries with low production costs, the RE PM rapidly covered most

of the market. Nevertheless, the situation changed dramatically around 2010, when the so-called RE-crisis struck [4]. With the industrial development of emerging countries (especially China), their requirements for PMs has increased substantially, and consequently, the prices of PMs has increased. Accordingly, an urgent need to find alternatives to RE PMs, especially in the intermediate energy product, BH_{max}, range between 50 and 200 kJ m^{-3} has emerged [5–7]. Therefore, novel, low-cost hybrid magnets based on ferrites/alnicos or any of their combinations with BH_{max}, between 50 and 200 kJ m^{-3} represent an interesting and viable solution to close the gap in the magnetic performance between ferrites and RE magnets [7]. One of the approaches to achieve enhancement of the energy product of already known and well-researched materials is the exploitation of magnetic interactions in composite materials prepared from (at least two) different magnetic phases [8–13]. Namely, hybrid magnets based on a high magnetisation material (soft phase) magnetically coupled (exchange or magneto-dipolar interactions) to a material with large anisotropy (hard phase) can result in a magnet with high BH_{max} values [8]. However, in order to achieve efficient exchange-coupling the size of the soft phase should not exceed two times the size of the domain wall width of the hard phase and both phases should be in close contact [8].

Spark plasma sintering (SPS) has gained interest as a consolidation technique also in the field of magnets [13–19] since it enables fast heating rates, lower sintering temperatures and shorter sintering times compared to conventional sintering [20, 21]. All this presents an option for densification of materials with no, or with a limited grain growth [20, 21], which would positively affect the size of both phases after consolidation. A direct application of uniaxial pressure during densification by SPS could positively impact the magnetic properties (especially on remanence) of hexagonally shaped grains by aligning them in the preferential orientation [22].

A vast number of research papers present various exchange-coupled composites [10, 23–27], but papers reporting increased BH_{max} values based on exchange-coupled hard–soft consolidated magnetic materials are scarce. The BH_{max} of 14.3 kJ m^{-3} for a hard–soft magnetic ceramic composite was reported by Roy and Kumar [11], in which they presented a hard–soft magnetic composite consisting of $BaCa_2Fe_{16}O_{27}$ as the hard phase and Fe_3O_4 as the soft phase. Jenuš *et al* [13] reported on Sr-ferrite/Co-ferrite bulk composites with BH_{max} of 26.1 kJ m^{-3}. Despite those composites promising properties, cobalt is still considered a critical raw material [28] and its saturation magnetisation is among the lowest of the spinel ferrites [29]. Moreover, the electrification of society is happening at the speed of light and new/hybrid magnets with a low carbon imprint would mean a significant step forward in reaching carbon neutrality. Our goal is to produce ferrite-based magnets with enhanced magnetic properties, contributing to a greener future.

In this paper, we present the magnetic performance of hard–soft hybrid sintered composites based on the combination of hydrothermally synthesised strontium hexaferrite (SFO) and $Zn_{0.2}Fe_{2.8}O_4$ (MP) nanoparticles with a cubic spinel structure. The average size of the soft nanoparticles is adequate to achieve the exchange coupling with the hard ferrite while its composition is optimised to be the largest in the family of Zn-doped ferrites [30]. Tailoring the magnetic properties of hard–soft ferrite magnets towards an increased maximum energy product was explored.

2. Experimental

2.1. Synthesis of powders

$SrFe_{12}O_{19}$ (SFO) particles were synthesised by the hydrothermal method adopted with some modifications by Primc *et al* [31]. Briefly, aqueous solutions of metal ions were prepared from strontium (II) nitrate ($Sr(NO_3)_2$, 99%, Across Organics, Thermo Fisher Scientific, Geel, Belgium) and iron (III) nitrate nonahydrate ($Fe(NO_3)_3 \times 9H_2O$, 98%, Carlo Erba Reagents (Peypin, France)) salts. The reagents were used as received, without any further purification. The exact metal concentration of the reagents was determined by chemical analyses (ICP–AES, PE OPTIMA 3100RL (Perkin Elmer Optima, Waltham, MA)). To the aqueous solution of Sr^{2+} and Fe^{3+}, with a Sr^{2+}/Fe^{3+} ratio of 1/6, the sodium hydroxide (NaOH, 98%, Alfa Aesar, Karlsruhe, Germany) aqueous solution was added at room temperature so that the NO_3^-/OH^+ ratio was 1/2. The mixture was then put into a stainless-steel autoclave and put in an oven pre-heated to 245 °C, kept at the temperature for 15 min and then cooled down to room temperature. The as-synthesised powder was additionally annealed at 1000 °C for 5 h.

Zn-doped ferrite (MP particles) was prepared through a co-precipitation synthesis, which is a low-cost, eco-friendly and industrially scalable approach. The stoichiometry of the soft ferrites was adjusted with the target to maximise the saturation magnetisation according to literature data [30]. In short, Zn^{2+} ($ZnCl_2$, ⩾98%, Sigma Aldrich), Fe^{2+} ($FeCl_2 \times 4H_2O$, 98%, Sigma Aldrich) and Fe^{3+} ($FeCl_3 \times 6H_2O$, 98%, Sigma Aldrich) amounts were adjusted accordingly to the desired stoichiometry. These synthesis details are reported in table S01 in the supporting information (available online at stacks.iop.org/JPD/54/204002/mmedia). In a typical synthesis, 40 g of NaOH (⩾98%, Sigma Aldrich) was solubilised in 1 l of N_2 purged demineralised (DM) water. The basic solution was heated up to reflux under vigorous stirring and N_2 flow. A solution of transition metals, prepared by solubilising the metal chlorides in 250 ml of N_2 purged DM water, was added quickly dropwise to the basic one at reflux, under vigorous stirring and N_2 flow.

The resulting black mixture was kept at reflux for 2 h, then cooled down to room temperature. The black precipitate was collected with the PM, washed several times with N_2 purged water, ethanol and acetone and dried under N_2 flow. The stoichiometries were checked through x-ray fluorescence spectroscopy (Rigaku Primus II, equipped with an Rh Kα radiation source and a wavelength dispersive detector) and always found equal to the nominal ones. In this study, the as-synthesised

Table 1. Selected hard and soft phase particles (names, composition, size and saturation magnetisation).

Name	Composition	Particles' size[a]	M_s Am^2 kg^{-1}
SFO	$SrFe_{12}O_{19}$	1 μm	59
MP	$Zn_{0.2}Fe_{2.8}O_4$	10 nm	85

[a]Determined by TEM or SEM analyses (see figure 2).

nanopowders without additional thermal treatment (sample MP) were used.

Powder mixtures of SFO and MP particles used for the consolidation were prepared in different ratios (SFO-xMP, $x = 5$ and 10 vol%, corresponding to 4.8 and 9.1 wt%, respectively) by mixing in isopropanol and homogenised with an ultrasonic processor VCX500 (Sonics & Materials Inc., USA) for 2 min at a power of 250 W, frequency 20 kHz and pulse on/off of 1 s. Basic properties of single phase materials used in this study are presented in table 1.

2.2. Consolidation

Prior to sintering, the powder mixtures were dispersed in isopropanol and oriented under an applied magnetic field of 0.5 T. The used mixtures were assembled in a graphite die, commonly used for SPS. In order to remove the solvent, the graphite die was placed in an oven at 80 °C and dried overnight. Powders were consolidated by SPS (Dr SINTER SPS SYNTEX 3000, Fuji Electronic Industrial) at 850 °C with a heating rate of 100 °C min^{-1}, holding times between 1 and 10 min and applied uniaxial pressure of 90 MPa. The sintered magnets had a cylindrical shape with a diameter of 10 mm and a thickness of approximately 2 mm.

2.3. Characterisation

The crystal structure of constituent powders and sintered samples were identified by x-ray diffraction (XRD, Siemens D5000 (Munich, Germany)) with the CuKa radiation. EVA and TOPAS softwares (Bruker AXS, Karlsruhe, Germany) were used for the analysis and refinement of obtained XRD data. The measuring step was 0.02° s^{-1} with a 4 s measuring time per step. The soft phase morphology and crystallinity were characterised using a transmission electron microscope (TEM) with an accelerating voltage of 200 kV (Jeol 2100, Tokyo, Japan). The powder microstructures and sintered composites were investigated with a field-emission scanning electron microscope (SEM; Jeol 7600F). Their chemical phase composition was determined with energy-dispersive x-ray spectroscopy (EDXS; Inca, Oxford Instruments Analytical Ltd, Abingdon, UK). The composites density after the SPS was calculated from the pellets dimensions and is presented in table 2.

The room-temperature magnetic properties of the powders were measured with a vibrating sample magnetometer (VSM; Lake Shore). The maximum energy product of sintered composites was determined with the permeameter (Steingroever EP2). Powders were oriented in an external magnetic field of 2 T prior to the magnetic characterisation. The anisotropy field (H_a) of selected SPS sintered single-phase and composite magnets were determined using the singular point detection (SPD) technique. SPD is a unique technique that allows measuring the H_a and metamagnetic transitions in polycrystalline materials directly [32]. The derivatives of magnetisation with respect to time are recorded when the sample is under a magnetic pulse. The pulse shape is recorded and the derivatives with respect to the magnetic field are obtained. In materials with uniaxial magnetocrystalline anisotropy, the second derivative d^2M/dH^2 features a peak at $H = H_a$, originated by the grains with an easy axis oriented perpendicularly to the magnetic field [32–35].

3. Results and discussion

The phase composition of the starting powders and powder mixtures determined by XRD, presented in figure 1, revealed that in the case of individual powders only peaks corresponding to the single-phase materials were present, while in the powder mixture peaks corresponding to both phases were detected. The hard phase powder (SFO) displayed sharp, well-defined peaks indicating a high degree of crystallinity. On the other hand, the XRD analysis of soft phase, MP, powder resulted in broader diffraction peaks typical for nanometric materials. XRD analyses also confirmed that prepared powder mixtures (for the sake of clarity is in figure 1 presented only one of them) consisted of selected phases in corresponding ratios. XRD patterns shown in figure 1 are also presented in supporting information as individual figures S2–S4 in which each samples diffractogram is compared to its calculated pattern. Phase analyses, which confirmed the composition of selected powders and powder mixtures, were followed by the electron microscopy (transmission and scanning) examination of selected starting powders and mixtures. The representative micrographs are presented in figure 2.

The morphology of starting hard phase powder analysed by SEM revealed SFO particles (figure 2(a)) with a diameter of approximately 1 μm and thickness of a few tens of nanometers (up to 100 nm). They had typical hexagonal shape and high diameter to thickness ratio. The average particles size of selected soft phase material was determined to be 10 nm. Their shape was irregular leaning towards spherical (figure 2(b)), which is a typical morphology for nanometric spinel ferrites.

Starting powders and mixtures were also characterised in terms of magnetic properties by VSM measurements in a random orientation and after orientation in an external magnetic field. The hysteresis loops presented in figure 3 represent single-phase materials, the effect of volume fraction and properties of soft phase on magnetic properties and shape of hysteresis loops. Soft phase particles (MP) displayed almost superparamagnetic behaviour with a very narrow hysteresis loop with saturation magnetisation (M_S) values of 85 Am^2 kg^{-1}. On the other hand, SFO displayed typical hard-ferrite magnetic properties with a coercivity (H_C) of slightly higher than

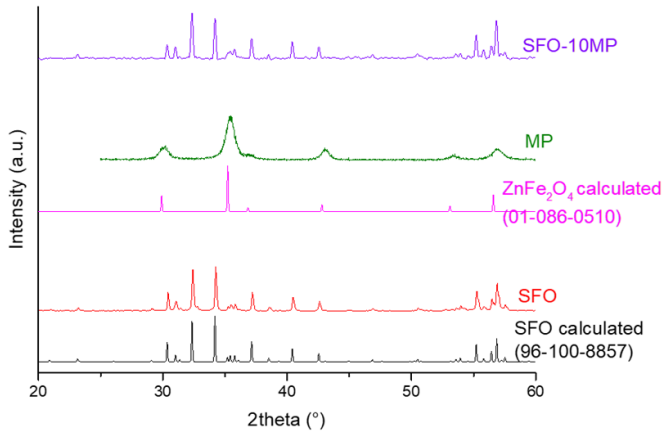

Figure 1. XRD diffractograms of starting powders, powder mixtures and corresponding reference patterns.

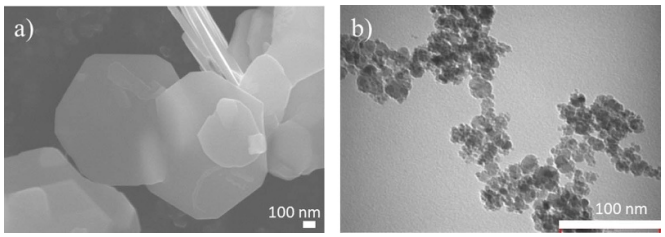

Figure 2. Electron microscopy (EM) micrographs of starting powders: (a) SEM of SFO and (b) TEM of MP.

300 kA m^{-1} and M_S of 59 Am^2 kg^{-1}. While 5 vol% of MP particles does not significantly affect either the magnetic properties or shape of the hysteresis loop of the hard–soft powder mixture, 10 vol% addition affects both the magnetic properties and shape of the hysteresis loop (figure 3). Namely, with an increasing amount of the soft phase in the mixture, the M_S increases (62 Am^2 kg^{-1} for the mixture with 10 vol% of the soft phase). The measured M_S values of powder mixtures are also in accordance with calculated M_S values for given composites, which are 60.3 Am^2 kg^{-1} for SFO-5MP and 61.4 Am^2 kg^{-1} for SFO-10MP, respectively. On the other hand, with an increase in the soft phase content H_C is decreasing (278 kA m^{-1} for the mixture with 10 vol% of the soft phase) and the knee in the hysteresis loop, characteristic for a physical mixture of hard and soft magnetic phase, is getting more and more pronounced. The latter was expected since particles of both phases were not in close contact in the prepared powder mixtures. The magnetic behaviour observed was caused by magnetic phases without an exchange interaction.

As described in section 2.2, powder mixtures were compacted by SPS at 850 °C with an applied pressure of 90 MPa and with holding times varying between 1 and 10 min. XRD analysis of sintered pellets was done on the polished pellets top surface, which is perpendicular to the applied magnetic field and pressing direction. The diffractograms of sintered SFO and SFO-10MP are presented in supporting information in figure S5. The phase analysis has revealed that during the processing and consolidation, the texturing occurred. Namely,

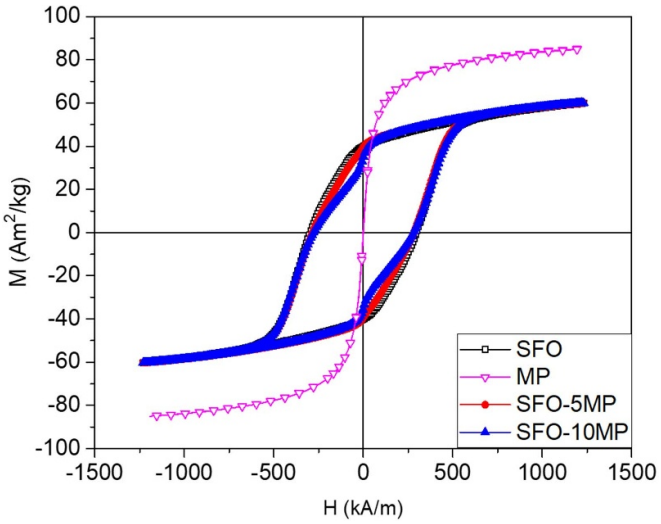

Figure 3. Hysteresis loops of starting single-phase powders and powder mixtures.

SFO particles used in this study had strongly anisotropic shape—thin hexagonal platelets with a diameter approximately ten times larger than its thickness. This, together with an applied magnetic field prior to the sintering and applied uniaxial pressure during the sintering, caused orientation of SFO platelets with its *c*-axis parallel to the applied magnetic field and pressure. The orientation of SFO particles is in XRD patterns shown as changes in the intensities or even absence of some characteristic *hkl* peaks with $l \neq 0$ [36–38]. The microstructural analysis of sintered samples was done on the fractured surfaces (on figure 4 denoted as 'Fractured surface—side view') and also on polished surfaces (on figure 4 denoted as 'Polished surface—top view'). The distribution of hard and soft phase in the composite is essential since the (in)homogeneity of phases influences magnetic interactions between both phases and magnetic properties of sintered composite magnets [23, 31]. Therefore, polished top surfaces of sintered samples were examined by EDXS elemental mapping analysis to determine the phase distribution after sintering. Since Fe and O are constituent elements in both, hard and the soft phase, it was expected that both elements are equally distributed in examined samples, and that was also the case here (supporting information, figure S6). The Zn and Sr maps (figure 4, bottom) are the ones that tell us the distribution of phases in the prepared composites. It can be seen that macroscopically the soft phase is relatively homogenously distributed in the hard phase matrix. However, despite the mixing of starting powders in the solvent by using a sonicator, the size of 'Zn islands' indicate an agglomeration of the soft phase particles, which could have a detrimental effect on magnetic properties of sintered composite magnets. The latter suggests that even mixing by sonication is not enough to break the agglomerates of nanoparticles formed in a powder. Although the use of nanoparticles in the form of stable suspensions is less favourable from the potential scale-up point of view, it would benefit to a more homogenous mixture of constituent phases.

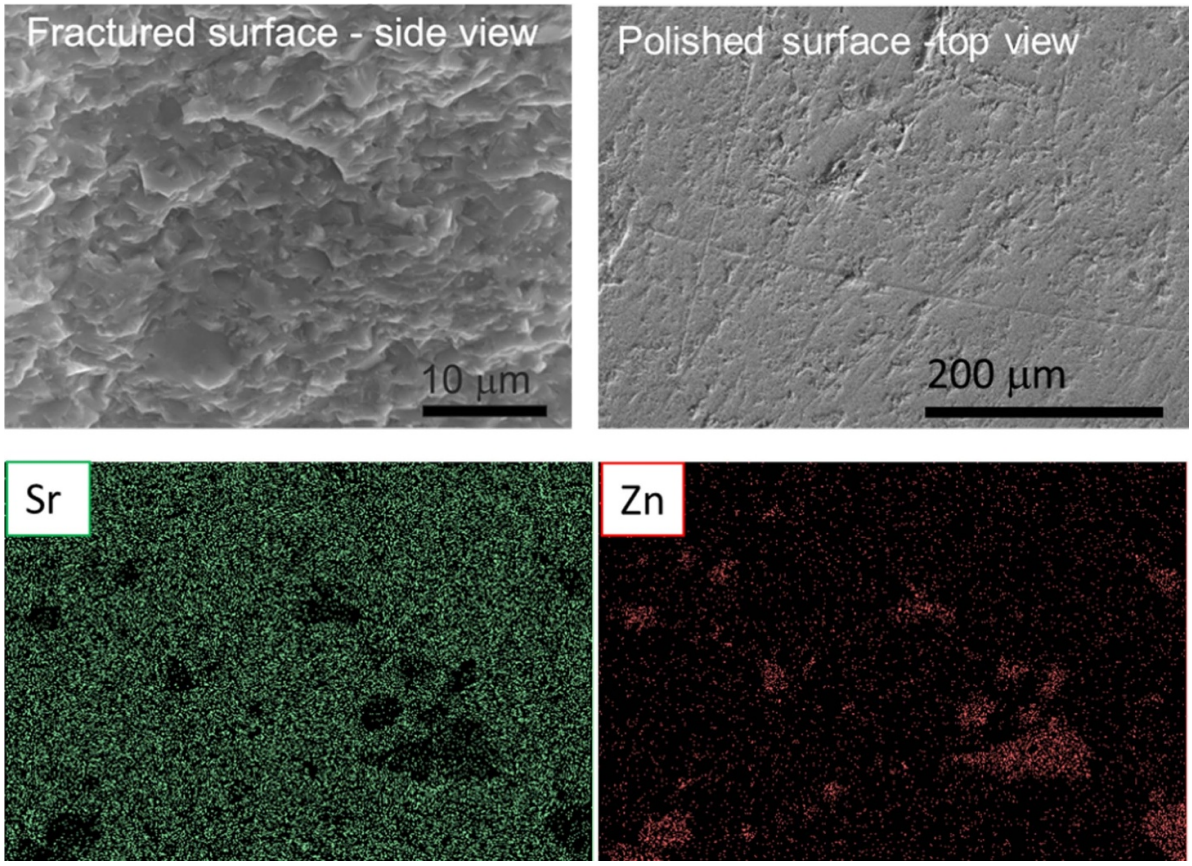

Figure 4. SEM micrographs of sintered composite SFO-10MP sintered at 850 °C for 5 min and applied pressure of 90 MPa, representing fractured surface, polished surface and corresponding EDXS elemental maps obtained on the presented polished surface. The scale bar for the maps is the same as for the 'polished surface' image.

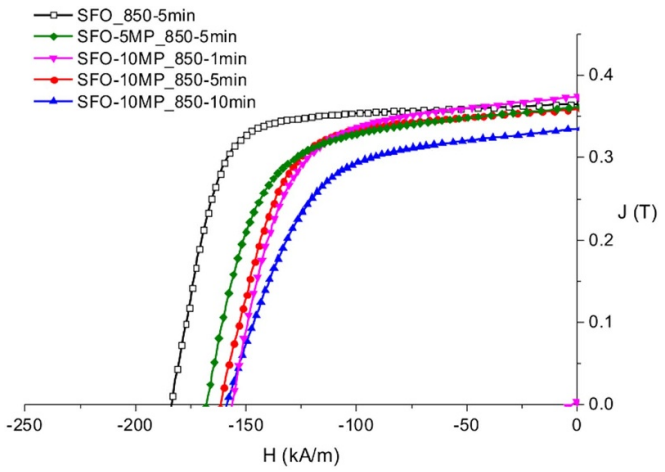

Figure 5. Demagnetisation curves of sintered magnets. Single-phase SFO sintered at 850 °C, 5 min, 90 MPa vs composites with 5 or 10 vol% of nanosized $Zn_{0.2}Fe_{2.8}O_4$ sintered at 850 °C, 90 MPa and different holding times.

To determine magnetic properties of sintered single hard-phase and composite magnets the demagnetisation curves were measured. Figure 5 represents a comparison between hard–phase SFO and SFO–MP composite magnets prepared under the same conditions. The corresponding remanence (B_R), coercivity (H_C), maximum energy product (BH_{max}) and sintered density (ρ) values are listed in table 2. It can be seen from figure 5 that single-phase SFO displays a square-like shape of the demagnetisation curve with the remanence of 365 mT and coercivity of 183 kA m^{-1}, leading to the BH_{max} of 23.9 kJ m^{-3}. Those magnetic properties are promising, but still lower than magnetic properties of currently available commercial sintered Sr-ferrite magnets ($B_R \sim 400$ mT and BH_{max} up to 40 kJ m^{-3}) [39]. Remanence of consolidated magnets also depends on the bulk piece's density, so one of the reasons for lower values can be found in the sintered densities of our material (4.84 g cm^{-3} or 94.5% of theoretical density). Although some orientation was observed in our samples, it was not enough to be compared to the industrial oriented ferrite magnets.

One way to improve the maximum energy product of magnets lies in a composite consisting of hard and soft magnetic phase with an exchange interaction between the phases. The theory of exchange interaction between hard and soft magnetic phases says that apart from being in close contact, the soft phase's size should not exceed a certain limit [8]. If the hard phase is Sr–ferrite, then this size is roughly 28 nm [29]. Therefore, the used soft phase material had an average particle size of 10 nm, which is well below the above-mentioned size

Table 2. Magnetic properties and density of selected SPS sintered magnets.

	B_r (mT)	H_c (kA m^{-1})	BH_{max} (kJ m^{-3})	ρ (g cm^{-3})
SFO	365.1	183.8	23.9	4.84
SFO-5MP_850-5 min	358.4	167.9	20.9	4.70
SFO-10MP_850-1 min	373.9	156.3	21.1	4.61
SFO-10MP_850-5 min	361	161.5	20.3	4.74
SFO-10MP_850-10 min	335	158.9	17.1	4.95

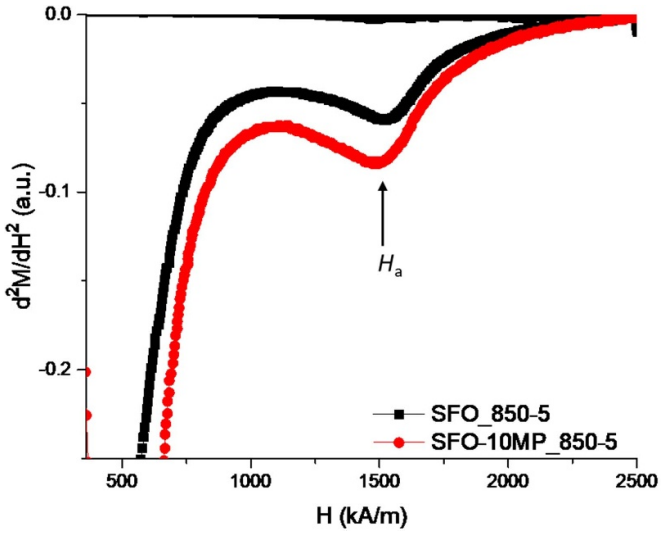

Figure 6. The second derivative of magnetisation of SFO and SFO-10MP magnets both sintered at 850 °C, 5 min and 90 MPa measured by singular point detection (SPD) technique.

limitation. While there was no substantial difference between the magnetic performance of composites with 5 or 10 vol% of soft phase (composites SFO-5MP and SFO-10MP) consolidated using the same sintering conditions (SPS, 850 °C, 5 min and 90 MPa), there was a decrease of magnetic properties, especially remanence, when longer holding times (SPS, 850 °C, 10 min and 90 MPa) were used. This indicates the beginning of the possible diffusion/reaction between magnetic phases or the reduction of the soft phase [40–42] leading to the deterioration of magnetic performance. Namely, a decrease in BH_{max} to 17 kJ m^{-3} was observed.

Although different sintered composite magnets varying soft phase composition and sintering conditions were prepared, none of the investigated samples displayed better magnetic properties than the single-phase Sr-ferrite. One of the reasons for this can probably be found in the (in)homogeneous distribution of both phases, possible diffusion between phases or in the reduction of the soft phase. That the later could also be a case in our study indicates the decrease in the magnetic properties when sintering time is prolonged (composite sintered for 10 min). Moreover, the addition of the soft phase can alter the shape of the demagnetisation curve leading to the reduction of the maximum energy product.

Selected samples were also investigated in terms of anisotropy field, H_a, by using the SPD technique [32, 35]. The H_a of ferrites depends on the magnetocrystalline anisotropy and the shape anisotropy [29]. However, an effective coupling between the hard and the soft phase in the composite would decrease the effective H_a compared to the pure hard phase [8]. The determination of H_a is even now a technical issue, being mainly possible in bulk monocrystals. In polycrystals and nanocrystals, H_a is calculated from the analysis of the approach-to-saturation law, from the transversal susceptibility or the radiofrequency measurements. By using SPD, however, the direct measurement of the H_a and metamagnetic transitions in polycrystalline materials is possible [32, 35]. Figure 6 represents the second derivative of magnetisation of SFO and SFO-10MP composite magnets sintered at 850 °C, for 5 min and applied pressure of 90 MPa. The H_a was determined as the minimum of the second derivative of the magnetisation at which the change of the magnetisation regime of grains with the easy axis oriented perpendicularly to the magnetic field occurred. H_a of single-phase SFO and SFO-10MP was little less than 1500 kA m^{-1}, both similar to the anisotropy field of bulk Sr-ferrite, which is 1432 kA m^{-1} [29]. No observable difference in the H_a of composites, when compared to the pure SFO, indicates that the exchange-coupling between the hard and the soft phase was not effective even though that particles were in close contact and that the size of the soft phase was within limits. This presumption is supported by the recently published paper by Soria *et al* [43] in which it was shown that for the effective coupling between the phases also a structural match must exist.

4. Conclusions

Ferrite-based composite magnets were prepared by sintering nanosized Sr-ferrite and Zn-ferrite by SPS. Depending on the concentration of the soft phase and sintering conditions, the magnetic properties of ferrite-based hybrid composites can be altered. The highest maximum energy product was determined for the single-phase Sr-ferrite. It was observed that longer sintering times (10 min) lead to the deterioration of hybrid composites' magnetic properties.

Acknowledgments

This work is supported by the European Commission through Project H2020 No. 720853 (AMPHIBIAN) and Slovenian Research Agency is acknowledged for funding the research program Ceramics and complementary materials for advanced engineering and biomedical applications (P2-0087), CEMM, JSI is acknowledged for the use of EM.

ORCID iDs

P Jenuš https://orcid.org/0000-0002-1926-479X
C Sangregorio https://orcid.org/0000-0002-2655-3901
M Petrecca https://orcid.org/0000-0002-4895-0254
M Albino https://orcid.org/0000-0001-7438-0833
C de Julián Fernández https://orcid.org/0000-0002-6671-2743
B Belec https://orcid.org/0000-0001-5286-1871

References

[1] Permanent Magnets 2020 Best Technology for Permanent Magnet Industry (available at: www.bestec4magnet.com/apply-tids-2.html) (Accessed 17 January 2020)
[2] Pavel C C, Lacal-Arántegui R, Marmier A, Schüler D, Tzimas E, Buchert M, Jenseit W and Blagoeva D 2017 Substitution strategies for reducing the use of rare earths in wind turbines *Resour. Policy* **52** 349–57
[3] Guerra M 2020 4 things you should know about magnets for electric vehicles (available at: www.electronicdesign.com/technologies/analog/article/21805919/4-things-you-should-know-about-magnets-for-electric-vehicles) (Accessed 24 January 2020)
[4] Bourzac K 2011 The rare–earth crisis *MIT Technol. Rev.* **114** 58–63
[5] Gutfleisch O, Willard M A, Brück E, Chen C H, Sankar S G and Liu J P 2011 Magnetic materials and devices for the 21st century: stronger, lighter, and more energy efficient *Adv. Mater.* **23** 821–42
[6] Lewis L H and Jiménez-Villacorta F 2013 Perspectives on permanent magnetic materials for energy conversion and power generation *Metall. Mater. Trans.* A **44** 2–20
[7] Coey J M D 2012 Permanent magnets: plugging the gap *Scr. Mater.* **67** 524–9
[8] Kneller E F and Hawig R 1991 The exchange-spring magnet: A new material principle for permanent magnets *IEEE Trans. Magn.* **27** 3588–600
[9] López-Ortega A, Estrader M, Salazar-Alvarez G, Roca A G and Nogués J 2015 Applications of exchange coupled bi-magnetic hard/soft and soft/hard magnetic core/shell nanoparticles *Phys. Rep.* **553** 1–32
[10] Mohseni F, Pullar R C, Vieira J M and Amaral J S 2019 Enhancement of maximum energy product in exchange-coupled $BaFe_{12}O_{19}/Fe_3O_4$ core-shell-like nanocomposites *J. Alloys Compd.* **806** 120–6
[11] Roy D and Kumar P S A 2009 Enhancement of (*BH*)max in a hard-soft-ferrite nanocomposite using exchange spring mechanism *J. Appl. Phys.* **106** 1–5
[12] Torkian S and Ghasemi A 2019 Energy product enhancement in sufficiently exchange-coupled nanocomposite ferrites *J. Magn. Magn. Mater.* **469** 119–27
[13] Jenuš P, Topole M, McGuiness P, Granados-Miralles C, Stingaciu M, Christensen M, Kobe S and Žužek Rožman K 2016 Ferrite-based exchange-coupled hard-soft magnets fabricated by spark plasma sintering *J. Am. Ceram. Soc.* **99** 1927–34
[14] Ovtar S, Le Gallet S, Minier L, Millot N and Lisjak D 2014 Control of barium ferrite decomposition during spark plasma sintering: towards nanostructured samples with anisotropic magnetic properties *J. Eur. Ceram. Soc.* **34** 337–46
[15] Mazaleyrat F, Pasko A, Bartok A and Lobue M 2011 Giant coercivity of dense nanostructured spark plasma sintered barium hexaferrite *J. Appl. Phys.* **109** 1–3
[16] Pullar R C 2012 Hexagonal ferrites: a review of the synthesis, properties and applications of hexaferrite ceramics *Prog. Mater. Sci.* **57** 1191–334
[17] Stingaciu M, Topole M, McGuiness P and Christensen M 2015 Magnetic properties of ball-milled $SrFe_{12}O_{19}$ particles consolidated by spark-plasma sintering *Sci. Rep.* **5** 14112
[18] Zhao W Y, Zhang Q J, Tang X F, Cheng H B and Zhai P C 2006 Nanostructural M-type barium hexaferrite synthesized by spark plasma sintering method *J. Appl. Phys.* **99** 99–102
[19] Obara G, Yamamoto H, Tani M and Tokita M 2002 Magnetic properties of spark plasma sintering magnets using fine powders prepared by mechanical compounding method *J. Magn. Magn. Mater.* **239** 464–7
[20] Kirchner R 2011 'FAST'—field assisted sintering technology basics, state of the art and future aspects *International Spring School on Field Assisted Sintering Technique (FAST) Darmstadt*
[21] Munir Z A, Anselmi-Tamburini U and Ohyanagi M 2006 The effect of electric field and pressure on the synthesis and consolidation of materials: a review of the spark plasma sintering method *J. Mater. Sci.* **41** 763–77
[22] Volodchenkov A D, Ramirez S, Samnakay R, Salgado R, Kodera Y, Balandin A A and Garay J E 2017 Magnetic and thermal transport properties of $SrFe_{12}O_{19}$ permanent magnets with anisotropic grain structure *Mater. Des.* **125** 62–68
[23] Belec B, Dražić G, Gyergyek S, Podmiljšak B, Goršak T, Komelj M, Nogués J and Makovec D 2017 Novel Ba-hexaferrite structural variations stabilized on the nanoscale as building blocks for epitaxial bi-magnetic hard/soft sandwiched maghemite/hexaferrite/maghemite nanoplatelets with out-of-plane easy axis and enhanced magnetization *Nanoscale* **9** 17551–60
[24] Cabreira-Gomes R, G. Silva F, Aquino R, Bonville P, Tourinho F A, Perzynski R and Depeyrot J 2014 Exchange bias of $MnFe_2O_4@\gamma Fe_2O_3$ and $CoFe_2O_4@\gamma Fe_2O_3$ core/shell nanoparticles *J. Magn. Magn. Mater.* **368** 409–14
[25] Granados-Miralles C, Quesada A, Saura-Múzquiz M, Andersen H L, Fernández J F and Christensen M 2020 Expanding the tunability and applicability of exchange-coupled/decoupled magnetic nanocomposites *Mater. Chem. Front.* **4** 1222–30
[26] Xu Y F, Ma Y Q, Xu S T, Zan F L, Zheng G H and Dai Z X 2014 Effects of vacancy and exchange-coupling between grains on magnetic properties of $SrFe_{12}O_{19}$ and α–Fe_2O_3 composites *Mater. Res. Bull.* **57** 13–18
[27] de Julian Fernandez C, Sangregorio C, de la Figuera J, Belec B, Makovec D and Quesada A 2021 Topical review: progress and prospects of hard hexaferrites for permanent magnet applications *J. Phys. D: Appl. Phys.* **54** 153001
[28] Keersemaker M 2020 Critical Raw Materials *Suriname Revisited: Economic Potential of its Mineral Resources* (Berlin: Springer) pp 69–82
[29] Smit J and Wijn H P J 1959 Ferrites (Eindhoven: Philips Technical Library) 369
[30] Petrecca M, Muzzi B, Olivieri S, Albino M, Yaacoub N, Peddis D, de Julian Fernandez C, Innocenti C and Sangregorio C 2021 Optimizing the magnetic properties of hard and soft materials for producing exchange spring permanent magnets *J. Phys. D: Appl. Phys.* **54** 134003
[31] Primc D, Makovec D, Lisjak D and Drofenik M 2009 Hydrothermal synthesis of ultrafine barium hexaferrite nanoparticles and the preparation of their stable suspensions *Nanotechnology* **20** 315605
[32] Asti G, Bolzoni F and Cabassi R 1993 Singular point detection in multidomain samples *J. Appl. Phys.* **73** 323–33

[33] Asti G, Solzi M, Bolzoni F and Albertini F 1995 Role of anisotropy on high field transitions in ferrimagnetic free particles *J. Magn. Magn. Mater.* **140–144** 1519–20
[34] Bolzoni F 1993 Magnetocrystalline anisotropy measurements in static or quasistatic magnetic fields *Rev. Sci. Instrum.* **64** 1569–75
[35] Cabassi R and Bolzoni F 2015 Canted-to-canted singular points in ferrimagnetic polycrystalline magnetization curves *J. Magn. Magn. Mater.* **390** 8–14
[36] Makovec D, Gyergyek S, Goršak T, Belec B and Lisjak D 2019 Evolution of the microstructure during the early stages of sintering barium hexaferrite nanoplatelets *J. Eur. Ceram. Soc.* **39** 4831–41
[37] Saura-Múzquiz M, Granados-Miralles C, Stingaciu M, Bøjesen E D, Li Q, Song J, Dong M, Eikeland E and Christensen M 2016 Improved performance of $SrFe_{12}O_{19}$ bulk magnets through bottom-up nanostructuring *Nanoscale* **8** 2857–66
[38] Drofenik M *et al* 2010 The concept of a low-temperature synthesis for superparamagnetic $BaFe_{12}O_{19}$ particles *J. Am. Ceram. Soc.* **93** 1602–7
[39] Hitachi Metals Ltd Permanent magnets—Hitachi
[40] Velinov N, Manova E, Tsoncheva T, Estournès C, Paneva D, Tenchev K, Petkova V, Koleva K, Kunev B and Mitov I 2012 Spark plasma sintering synthesis of $Ni_{1-x}Zn_xFe_2O_4$ ferrites: Mössbauer and catalytic study *Solid State Sci.* **14** 1092–9
[41] Sutka A, Stingaciu M, Jakovlevs D and Mezinskis G 2014 Comparison of different methods to produce dense zinc ferrite ceramics with high electrical resistance *Ceram. Int.* **40** 2519–22
[42] Valenzuela R, Gaudisson T and Ammar S 2016 Severe reduction of Ni–Zn ferrites during consolidation by spark plasma sintering (SPS) *J. Magn. Magn. Mater.* **400** 311–4
[43] Soria G D *et al* 2021 Uncorrelated magnetic domains in decoupled $SrFe_{12}O_{19}$/Co hard/soft bilayers *J. Appl. Phys.* **54** 054003